A Kinetic Investigation of the Catalytic Partial Oxidation of Propylene over a Rh/Al_2O_3 Catalyst

Davide Pagani, Dario Livio, Alessandro Donazzi, Matteo Maestri, Alessandra Beretta,* Gianpiero Groppi,* and Pio Forzatti

Laboratory of Catalysis and Catalytic Processes Dipartimento di Energia, Politecnico di Milano Piazza Leonardo da Vinci 32, Milano 20133, Italy

1. INTRODUCTION

The catalytic partial oxidation (CPO) of hydrocarbons is a promising technology for the small scale production of H_2 from a wide variety of fuels, including NG, LPG, logistic transportation fuels (such as gasoline, kerosene, diesel[1−3]) and biomass-derived fuels; it can be carried out under autothermal conditions, at millisecond contact time, in small and compact reactors.[1−9]

CH_4 CPO over Rh catalysts is unanimously recognized as a clean process; indeed no appreciable C-formation was detected by Raman spectroscopy from CH_4 CPO experiments[10] over Rh/Al_2O_3 layers. However, in the case of liquid fuels, the formation of C-deposits on the catalyst and downstream from the reactor is expected to be a critical issue. On the one side, the onset of homogeneous reactions can give rise to the formation of short olefins (precursors of polyaromatic species); on the other side, catalytic cracking reactions can form C-aggregates resistant to steam reforming reactions.

Deutschmann and co-workers[11−13] have studied the influence of gas-phase reactions on the catalytic reforming of isooctane on Rh-coated monoliths. Their modeling results showed that coke formation was strictly dependent on the C/O ratio and flow rate. At fuel-rich conditions gas-phase reactions formed a wide spectrum of hydrocarbon species (ethylene, acetylene, C_3−C_4 olefins, and aromatic molecules), which were responsible for coke formation after the oxidation zone. Adsorbed carbon atoms were predicted to increasingly cover the Rh catalyst under fuel-rich conditions and lead to the formation of a full monolayer of carbon.

Recently, Horn and co-workers[14] gave evidence for a substantial catalytic formation of surface carbon in methane CPO on polycrystalline platinum foils. By means of in situ Raman spectroscopy, they found that defective and inhomogeneous carbon species were produced right after reaction light-off and, depending on time on stream, the amorphous carbon compounds were both removed by oxidation and steam reforming and transformed into ordered graphite-like species. Additionally, the carbon deposition was found to be unevenly distributed on the Pt foil.

The same authors investigated methane CPO also on Pt-coated foam monoliths by means of spatially resolved measurements of temperature and composition.[15] The observed species profiles revealed two different zones along the axial coordinate. In the first zone, the rate of reactant conversion was fast; in the second zone (where O_2 conversion was almost complete), the consumption rate was much slower, associated with a change of the axial distribution of Pt and the formation of carbon deposits. This was confirmed by postreaction characterization of the catalyst by Raman spectroscopy. They also carried out a numerical analysis of the experiments by applying two different microkinetic schemes.[16,17] Even though both the schemes do not incorporate a mechanism of carbon growth, the simulations

Special Issue: Recent Advances in Natural Gas Conversion

Received: August 2, 2013
Revised: November 5, 2013
Accepted: November 11, 2013
Published: November 11, 2013

confirmed that the axial change of the rate of reactant conversion could be explained by a surface enrichment of CH_x* and C* intermediates.

In a previous investigation we applied the spatially resolved sampling technique to characterize the concentration and temperature profiles along a Rh-coated propane CPO reformer.[18,19] We found that short olefins are formed by homogeneous reactions in the inlet portion of the monolith channels and are subject to consecutive steam reforming on the catalyst surface. Bell-shaped concentration profiles were in fact measured for ethylene and propylene. To better understand the impact of short olefins on the kinetics of syngas production and the formation of C, we have analyzed the reactivity of propylene CPO and the surface abundance of C-species by combining activity tests in an isothermal annular microreactor with Raman and TPO measurements.[10] Rather unique reactivity features were found: C_3H_6 oxidation started at 200 °C, that is at much lower temperatures than the oxidation of other light hydrocarbons as CH_4 and C_3H_8 on Rh under fuel-rich conditions; the conversion of propylene leveled off in between 300 and 450 °C; the effective production of H_2 and CO started at 450−500 °C (at much higher temperature than the steam reforming of CH_4 and propane on Rh) and it steadily increased with temperature. The ex-situ Raman/TPO characterization after CPO tests showed that the surface was clean at the lowest temperature, where gaseous O_2 was still available, but disordered C-structures were formed on the surface at intermediate temperature. At increasing temperature up to 800 °C it was observed that the relative abundance of amorphous carbon deposits decreased, in favor of graphitic-like forms and even nanotubes.

On a qualitative basis, these pieces of evidence suggest that the adsorption of propylene may have an important role: a stronger adsorption of propylene compared to that of methane and propane could be invoked to justify the higher oxidation rate, the same strong adsorption in the absence of O_2 (the origin of the abundance of surface C detected by the Raman measurements) could be responsible for the inhibition of steam reforming at intermediate temperatures.

In this work, we extend the kinetic investigation on the partial oxidation of propylene on Rh, aiming at the development of a kinetic scheme of the process. A quantitative analysis of data collected in an annular reactor is performed to identify the main kinetic features as well as to describe a "C-poisoning" effect. Both lumped and microkinetic approaches were adopted. The lumped approach offers the advantage of an immediate identification and representation of the main kinetic dependences that govern the global reaction; the global rate expression is a flexible engineering tool, especially useful for reactor design applications. The detailed microkinetic approach offers instead a deeper insight of the surface chemistry, which is behind the macroscopic observation; this can be especially informative on the mechanism of the hydrocarbon activation, the nature of the most abundant surface intermediates, and in general the role of surface coverage effects, which are pivotal in the activation of functionalized molecules such as propylene.

2. EXPERIMENTAL AND MODELING

2.1. Catalyst Preparation and Characterization. α-Al_2O_3 (12 m^2/g) was used as a thermally stable support. It was obtained by calcination in air at 1100 °C for 10 h of commercial γ-Al_2O_3 (Puralox Sba-150, Sasol). Phase composition was verified by XRD. BET surface area amounted to about 10 m^2/g, with a pore volume of 0.2 cm^3/g.

All the experiments were carried out on a 2 wt % Rh/α-Al_2O_3 catalyst, which was prepared by dry impregnation of the α-Al_2O_3 support with an aqueous solution of $Rh(NO_3)_3$. For testing in the annular reactor, a total weight of 12 mg of catalyst was deposited in the form of a thin layer (35 μm), 2 cm long, on an alumina tubular support by a dip-coating standard procedure. A slurry was prepared by adding the catalyst powders to an acidic solution (HNO_3/powder = 1.7 mmol/g; H_2O/powder = 1.7 g/g). This mixture was ball-milled for 24 h. Finally, the ceramic tubes were coated by dipping them into the slurry, then extracting them at constant velocity. Rh loadings were verified by atomic absorption, while a pulse chemisorptions technique was applied to evaluate the dispersion of Rh, which was estimated at ∼20%. Details of the catalyst preparation and support characterization were reported elsewhere.[20]

2.2. Testing Apparatus and Operating Conditions. CPO and steam reforming (SR) experiments were performed in an annular reactor, which consists of the catalyst-coated alumina support (o.d. 4 mm) coaxially inserted into a quartz tube (i.d. 5 mm), giving rise to an annular duct (0.5 mm channel height), through which the gas flows in laminar regime due to the small channel opening. Because of the limited amount of catalyst (typically 10−15 mg), the reactor can operate at very high space velocity even at moderate flow rates; GHSV can easily range from 10^6 to 10^7 L(NTP)/(kg_{cat}/h). This allows a larger useful temperature window for the kinetic investigation, which is a highly desirable feature for studying the kinetics of very fast catalytic processes, at intermediate conversion of the reactants, far from thermodynamic control. Indeed, the annular reactor has been successfully applied in the past to investigate the kinetics of methane partial oxidation[21,22] and propane partial oxidation[23] over Rh/Al_2O_3. Another attractive characteristic of the annular reactor is the possibility to measure the axial temperature profile of the catalyst layer by simply sliding a thermocouple inside the internal ceramic tube. Dilution of the reacting mixture and efficient heat dissipation by radiation allow the temperature gradients to remain below 5 °C/cm thus realizing quasi-isothermal conditions.[24]

In this work, the feed gases were supplied by high pressure cylinders and low pressure mass flow controllers (Brooks Smart 5850S). A micro-GC (3000 A, Agilent Technologies) was used to analyze the inlet and the outlet gas compositions using N_2 as an internal standard. H_2O for SR tests was produced by the oxidation of a stoichiometric mixture of H_2 and O_2 diluted in N_2, in a separate reactor placed upstream of the annular reactor. This solution allowed a good control in H_2O feed that remained constant during the entire experimental run.

All the tests herein presented were performed at atmospheric pressure and at a gas hourly space velocity (GHSV) of 2×10^6 NL/(kg_{cat}/h), feeding a total flow rate of 400 Ncm^3/min (corresponding to a linear velocity of about 2.6 m/s and *Re* number of 30 at 500 °C). A typical run consisted of steady-state measurements at oven temperatures that varied from 200 up to 850 °C, with stepwise increments of 10−50 °C. Prior to the kinetic tests, the catalyst underwent a standard conditioning procedure, developed and discussed in a previous study.[20] Periodically, C_3H_6 CPO standard tests were performed in order to verify possible loss of activity of the catalyst.

2.3. Reactor Model and Thermodynamic Equilibrium Calculations. A 1D, heterogeneous model of the annular

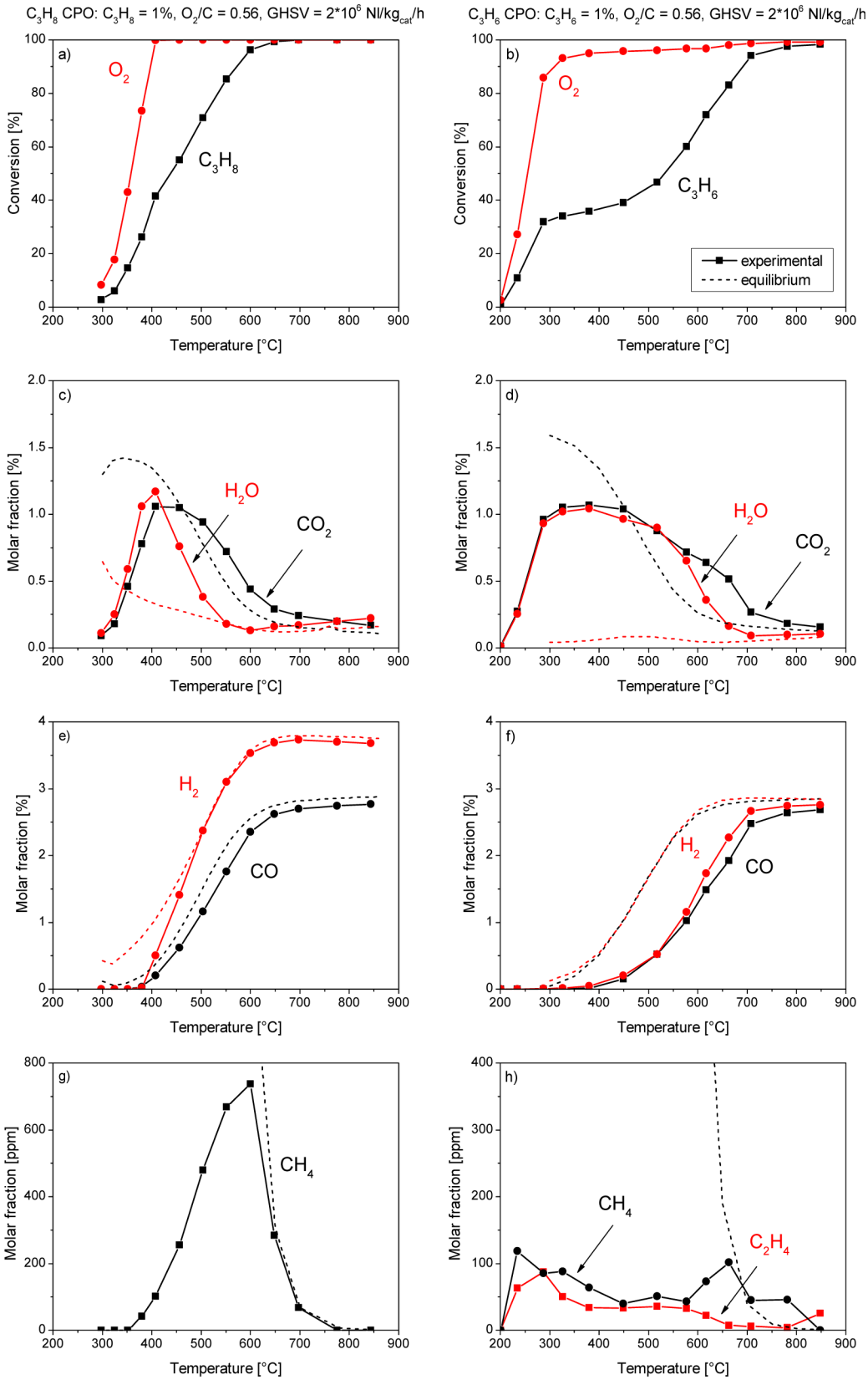

Figure 1. Comparison between CPO of propane (left) and propylene (right) on reactants and products. Experimental conversion and molar fractions are reported. Adapted with permission from D. Pagani, D. Livio, A. Donazzi, A. Beretta, G. Groppi, M. Maestri, E. Tronconi. A kinetic analysis of the partial oxidation of C_3H_8 over a 2% Rh/Al_2O_3 catalyst in annular microreactor. *Catal. Today*, 2012, *197*, 265–280. Copyright 2012 Elsevier and from A. Donazzi, D. Pagani, A. Lucotti, M. Tommasini, A. Beretta, G. Groppi, C. Castiglioni, P. Forzatti, P. Annular reactor testing and Raman surface characterization in the CPO of methane and propylene. *Appl. Catal. A: Gen.* 2013; http://dx.doi.org/10.1016/j.apcata.2013.06.005. Copyright 2013 Elsevier.

reactor was used for the quantitative analysis of the experimental results. The model consists of the mass balances of the reacting species in the gas phase and at the gas−solid interface. The measured axial profile of temperature was used as input in the simulations. External mass transfer limitations were accounted for by specific correlation of transport coefficients for laminar flow in annular ducts.[25] Internal diffusive resistances were taken into account by a generalized effectiveness factor. This was calculated for O_2 and C_3H_6; the effectiveness factor of O_2 was calculated based on the overall consumption rate of O_2 by oxidation of H_2, CO, and C_3H_6, while the effectiveness factor of C_3H_6 was calculated on the basis of the steam reforming rate of C_3H_6. Governing equations and details about the mathematical model can be found elsewhere.[21] A specific Rh surface of ∼1300 cm^{-1} was used as input in the simulation. This value was estimated based on the catalyst weight (12 mg), the Rh load (2%), and the Rh dispersion (20%), which were experimentally determined (see section 2.1).

The reactor model incorporates both lumped and microkinetic schemes for the CPO of light hydrocarbons on Rh. The original CH_4 lumped scheme, consisting of global equation rates expressed per unit catalyst weight was developed by Donazzi et al.[21,22] on the basis on an extensive investigation of CH_4 CPO in the annular reactor, and it consists of kinetic expressions for CH_4 total oxidation, CH_4 steam reforming, WGS and its reverse, H_2 and CO postcombustion. By adding rate equations for C_3H_8 total oxidation, C_3H_8 steam reforming and CO methanation, the kinetic scheme was extended to a description of C_3H_8 CPO.[23]

A thermodynamically consistent C_1 microkinetic scheme was also developed.[26,27] It consists of 82 elementary surface reactions and 13 adsorbed species, with equation rates expressed per unit Rh surface. The scheme was derived by using a hierarchical multiscale methodology involving both the semiempirical method (UBI-QEP) and first principles technique.[26,28] The model was validated over a comprehensive set of experimental data and it is capable of describing several reacting systems, including CH_4 steam reforming, dry reforming, partial oxidation, WGS, RWGS, H_2 and CO oxidation. In this work, a specific Rh surface of ∼1300 cm^{-1}, defined as (exposed Rh atoms surface)/(reactor volume)[cm^2/cm^3], was used as input in the simulation. This value was estimated on the basis of the catalyst weight (12 mg), the Rh load (2%), and the Rh dispersion (20%), which were experimentally determined (see section 2.1).

Thermodynamic equilibrium calculations for the C_3H_6/O_2 reacting system were performed at constant temperature and pressure by the STANJAN equilibrium code.[29] C_3H_8, C_3H_6, C_2H_6, C_2H_4, CH_4, O_2, N_2, CO, CO_2, H_2, and H_2O were considered at the equilibrium. Equilibrium calculations performed considering graphitic carbon (not reported), reveal that the formation of C is thermodynamically favored at low temperature, below 620 °C in the tests with O_2/C ration equal to 0.56 and below 500 °C in the tests with O_2/C ration equal to 1.

3. RESULTS

3.1. The Reference Case of Propane CPO in Annular Reactor. The CPO of saturated light hydrocarbons and in particular propane and methane has been broadly discussed in the literature.[21,22,30] In our experience,[21,23] the reactivity patterns of CH_4 and C_3H_8 are very similar and show the same prevailing kinetic dependences of the surface reactions. A detailed kinetic investigation of partial oxidation of C_3H_8 has been reported in a previous paper;[23] herein we propose a brief summary of the main results on C_3H_8 CPO as a reference case for better appreciating the findings from the propylene tests.

Figure 1 (panels on the left) reports the results of a standard C_3H_8 CPO test with a diluted feed stream (C_3H_8 = 1%, O_2/C = 0.56, N_2 to balance), in the temperature range 300−850 °C and gas space velocity of 2×10^6 NL/(kg_{cat}/h). The conversion of reactants and the molar fraction of products are plotted against the catalyst average temperature. Total oxidation of C_3H_8 started at about 300 °C; H_2O and CO_2 were the only detectable products up to about 400 °C, at which temperature the conversion of O_2 was complete. At this temperature the propane conversion curve showed a change of slope, caused by the transition from the oxidation regime to the combined oxidation plus reforming regime.[31] In fact, at increasing temperature, a decrease of H_2O molar fraction was observed, while CO and H_2 production increased steadily with the progress of C_3H_8 consumption. Reverse water gas shift also influenced the evolution of CO_2 with temperature. At low temperature CO and CO_2 methanation reactions were responsible for the production of methane (Figure 1g), whose concentration passed through a maximum at about 600 °C, and decreased at higher temperatures according to the thermodynamic equilibrium.

Experiments at varying O_2/C ratios clearly showed that the oxidation rate was independent of O_2 concentration. In analogy with that reported by Chin et al.[32] and Garcia-Diéguez et al.[30] on the activation of methane and ethane on Pt at high O/C ratios (Regime 1), such kinetic dependency can be explained by invoking that the breaking of the first C−H bond occurs on a surface saturated by chemisorbed O* atoms. Same kinetic features were found also for CH_4 activation on Rh.[21]

At increasing temperature, O_2 is rapidly consumed and free Rh sites become available for the steam reforming of C_3H_8 with production of CO and H_2. In a dedicated study the intrinsic rate of the reaction was found to be proportional to the fuel concentration and independent from the H_2O feed concentration.[23] This is in line with Regime 4 according to Iglesia and co-workers,[32,33] in which the rate determining step of CH_4 activation on Pt and Rh is the breakage of the first C−H bond on a vacancy−vacancy site pair.

3.2. Propylene CPO in Annular Reactor. Figure 1 (panels on the right) shows the results of a standard propylene CPO test, performed under the same operating conditions as the propane CPO test. The reaction between C_3H_6 and O_2 started at a temperature as low as 200 °C with formation of CO_2 and H_2O. The rate of C_3H_6 oxidation was so high that O_2 conversion was nearly complete (>90%) already at 300 °C. In this low temperature region, the formation of small amounts of CH_4 and C_2H_6 was also observed. This appeared as evidence of some catalytic cracking of C_3H_6, adsorbed on the surface. Despite the extremely high rate of oxidation, the reforming activity of propylene was apparently delayed at much higher temperatures than what was observed for propane. In fact, in between 300 and 450 °C the temperature sensitivity of the C_3H_6 conversion was very low, showing a sort of plateau. Only above 450 °C did the conversion of C_3H_6 proceed with increasing temperature, accompanied by the consumption of H_2O and the formation of CO and H_2 until reaching the equilibrium composition at about 800 °C. An ex situ Raman investigation combined with TPO measurements[10] revealed that at the intermediate temperatures where the conversion of

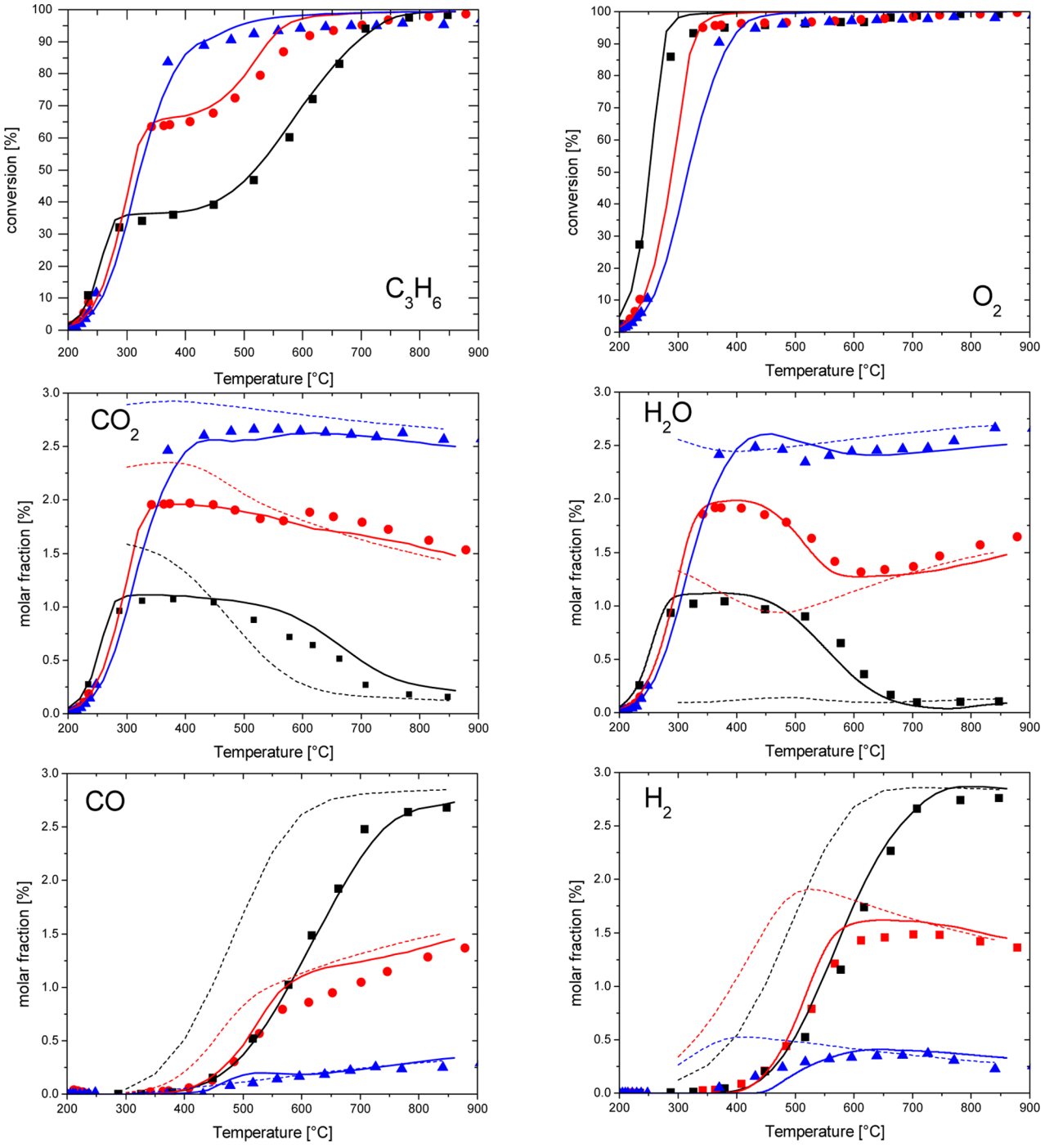

Figure 2. CPO tests at varying O_2 concentration. Experimental data (symbols), model simulations (solid lines), and equilibrium values (dashed lines) are reported. Operating conditions: C_3H_6 = 1%−3%, (■) O_2 = 1.7%, (●) O_2 = 3%, (▲) O_2 = 4%, N_2 to balance, GHSV = 2×10^6 NL/(kg_{cat}/h), atmospheric pressure.

the olefin leveled off, the surface was rich with C-species, mainly amorphous; these were believed to block the surface sites producing a poisoning effect. The coverage of C-species decreased (and their morphology changed) with increasing temperature where the steam reforming activity was recovered.

3.3. Tests of Propylene CPO at Varying O_2 and C_3H_6 Concentration. CPO tests were carried out at 1% v/v C_3H_6 inlet fraction, GHSV = 2×10^6 NL/(kg_{cat}/h) and increasing the O_2 inlet concentration in the range 1.7%−4% v/v. The conversion of the reactants and the molar fractions of the products are plotted against the average catalyst temperature in Figure 2. In the low temperature region (<250 °C), the conversion of propylene decreased with increasing O_2 concentration, indicating competitive adsorption of O_2 with propylene; coherently, the molar fraction of CO_2 and H_2O decreased. At medium temperature (250−400 °C) because of the increasing O_2 concentration, the fraction of propylene involved in deep oxidation to CO_2 and H_2O grew. Thus, the formation of the plateau was shifted at higher values and the residual amount of fuel available for reforming reactions was reduced. However, at 450−500 °C the rate of syngas production, though limited, was very similar in three experi-

ments indicating that the rate of steam reforming depends negligibly on C_3H_6 partial pressure. At high temperatures, coherently with thermodynamic equilibrium, syngas selectivity decreased with increasing O_2 concentration.

Additional tests were carried out with an O_2 inlet fraction of 1.68% v/v, GHSV of 2×10^6 NL/(kg_{cat}/h), by varying the concentration of C_3H_8 from 0.5% to 1.5% v/v. The experiments spanned a much more limited temperature range (200−250 °C), focusing on the kinetics of propylene oxidation. The conversion of the reactants is plotted in Figure 3 as a function

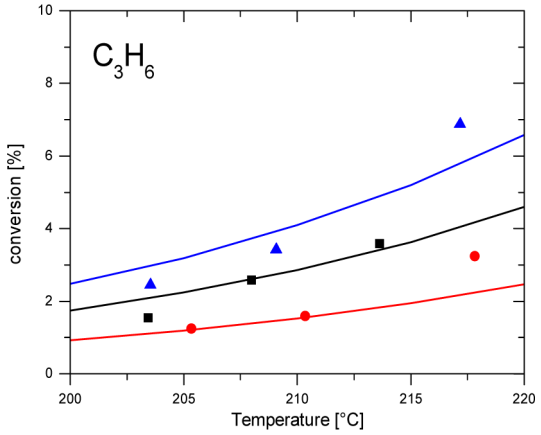

Figure 3. CPO tests at varying C_3H_6 concentration, experimental (symbols) and calculated (solid lines). Operating conditions: (▲) C_3H_6 = 1.5%, (■) C_3H_6 = 1%, (●) C_3H_6 = 0.5%, O_2 = 1.68%, N_2 to balance, GHSV = 2×10^6 NL/(kg_{cat}/h), atmospheric pressure.

of the average catalyst temperature. The conversion of C_3H_6 increased with the hydrocarbon concentration indicating a kinetic order greater than 1 on C_3H_6 concentration.

3.4. Steam Reforming. SR tests were carried out at GHSV at 2×10^6 NL/(kg_{cat}/h) in the temperature range 300−850 °C, varying the concentration of H_2O from 2% to 3%, while the amount of C_3H_6 was kept constant at 0.5%. The results are plotted in Figure 4. It was observed that the conversion of C_3H_8 increased with the increasing of H_2O concentrations indicating a positive order on H_2O concentration.

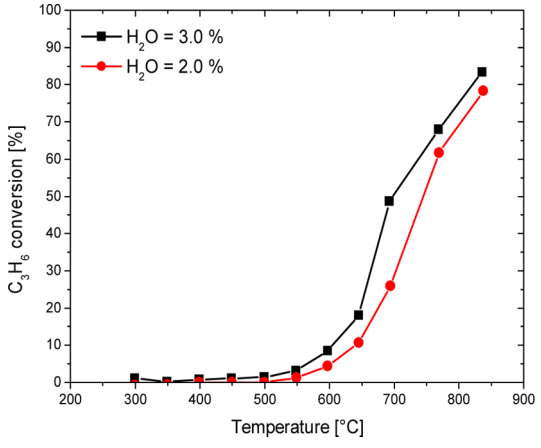

Figure 4. Test of propylene SR at varying H_2O concentration. Operating conditions: C_3H_8 = 0.5%, (●) H_2O = 2%, (■) H_2O = 3%, N_2 to balance, GHSV = 2×10^6 NL/(kg_{cat}/h), atmospheric pressure.

4. LUMPED KINETIC ANALYSIS

Data were analyzed with the same lumped approach as the one adopted for describing the kinetics of CH_4 and C_3H_8 CPO by Donazzi et al.[21,22] and Pagani et al.,[23] respectively. The kinetic scheme reported in those papers was herein extended to incorporate rate expressions for the global reactions of propylene oxidation and propylene steam reforming. In propylene CPO, additional global reactions are involved including WGS, reverse-WGS, CO and H_2 postcombustion, and CO methanation; these were not adapted to the present data, but imported from our previous kinetic studies. The rate expressions used for total oxidation and steam reforming of propylene are discussed in the following. The values of the kinetic parameters estimated by model fitting to the present data are reported in Table 1. The overall response of the model is shown by the solid lines in Figures 2 and 3 and appears largely satisfactory.

4.1. Total Oxidation. All the CPO tests characterized by incomplete conversion of O_2 (<95%, i.e., at temperatures below 250 °C) were treated as C_3H_6 total oxidation data. Thus, they were used to derive the kinetic expression of propylene oxidation. First, turnover rates (TOR) were evaluated from differential data (T < 225 °C), accounting for the number of exposed Rh atoms, which was evaluated by correcting the effective Rh load by the estimate of Rh dispersion. In Figure 5, TOR are plotted at varying propylene (Figure 5a) and O_2 (Figure 5b) molar fractions. Looking at the slope of the logarithmic plot it is evident that the intrinsic rate of oxidation has an inverse dependence on O_2 concentration, while it shows a quadratic dependence on propylene concentration.

We thus propose that the activation of C_3H_6 in the presence of O_2 occurs in a kinetic regime similar to the one that Chin et al.[32,34] have identified as Regime 2 on Pt, wherein the catalyst surface is not fully saturated by O* species and the activation of the hydrocarbon occurs on highly reactive site pairs that couple one vacancy and one chemisorbed oxygen atom (*−O*). As detailed in the original papers by Iglesia and co-workers, the quadratic dependence on the hydrocarbon and the negative dependence on O_2 are explained by the assumption that the rate determining step of propylene activation is the dissociative adsorption on the vacancy-O* pair, together with the assumption of irreversible dissociation of O_2* (adsorbed molecular oxygen) into atomic O*; these assumptions lead in fact to the following rate expression:

$$r_{C_3H_6Ox} = \frac{k_{Ox} P_{O_2}}{\left(1 + K_1 \frac{P_{O_2}}{P_{C_3H_6}}\right)^2} \quad (1)$$

Equation 1 was adapted to the entire set of oxidation data. It turns out that the term in the denominator $K_1(P_{O_2}/P_{C_3H_6})$, originating from the balance of O* sites, is much larger than 1, confirming that, at low temperature, where propylene oxidation occurs, O* is the most abundant surface intermediate (MASI). In practice, the reaction rate could be expressed in the simplified form:

$$r_{C_3H_6Ox} = \frac{k_{Ox} P_{C_3H_6}^2}{K_1^2 P_{O_2}} \quad (2)$$

Thus, in the case of the olefin, differently from the case of C_3H_8 (or CH_4), free Rh sites become available and originate highly reactive *−O* pairs; indeed, the comparison between propane

Table 1. Rate Equations[a] and Parameter Estimates for C_3H_6 Total Oxidation and Steam Reforming Added to the Molecular Kinetic Scheme by Pagani et al.[23]

reaction	rate [mol g_{cat}^{-1} s^{-1}]	k_0 [mol atm^{-1} g_{cat}^{-1} s^{-1}]	E_a [kJ mol^{-1}]
$C_3H_6 + \frac{9}{2}O_2 \rightarrow 3CO_2 + 3H_2O$	$r_{C_3H_6Ox} = \frac{k_{Ox}P_{O_2}}{\left(1 + K_1\frac{P_{O_2}}{P_{C_3H_6}}\right)^2}$	32.09	54
$C_3H_6 + 3H_2O \leftrightarrow 3CO + 6H_2$	$r_{C_3H_6SR} = \frac{k_{SR}P_{C_3H_6}}{1 + K_2\frac{P_{C_3H_6}}{P_{H_2O}}}(1 - \eta_{C_3H_6SR})$	10.49	76
where $K_1 = 1.4\exp\left[-\frac{22000}{R}\left(\frac{1}{T} - \frac{1}{T_0}\right)\right]$ and $K_2 = 78\exp\left[-\frac{42000}{R}\left(\frac{1}{T} - \frac{1}{T_0}\right)\right]$			

[a]The reaction rate constant (k) is calculated as $k = k_0 \exp[-(E_a/R)\cdot((1/T) - (1/T_0))$, where k_0 is the pre-exponential factor estimated at the reference temperature, T_0 = 873 K.

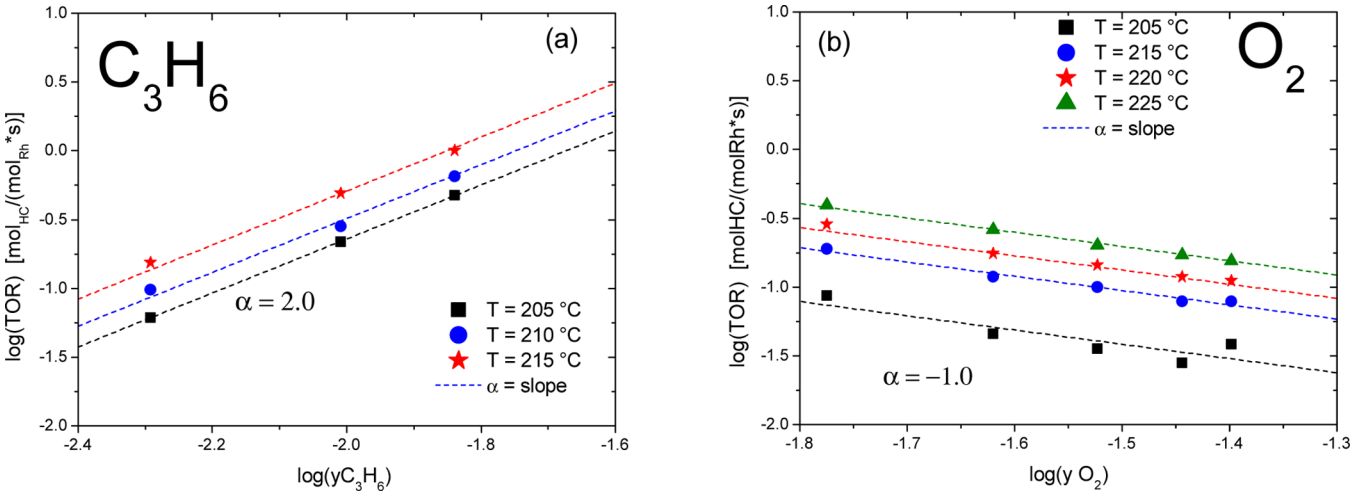

Figure 5. (a) Turnover rates at increasing C_3H_6 molar fraction, (b) turnover at increasing O_2 molar fraction.

oxidation and propylene oxidation on Rh involves not only a change of the kinetic dependences, but also a sharp increase of TOR. This is also fully in line with the findings of Chin et al.,[32,34] who have shown a great increase of the TOR from Regime 1 to Regime 2 and have theoretically explained it based on the concerted effect of the vacancy-O* pair in stabilizing the transition state of the C−H cleavage step (with formation of a *−C−H−O* species). This behavior is likely due to the affinity of the olefin with the surface, which strongly adsorbs by π-bonding on Rh sites,[35,36] thus leading to an effective competition with O_2 adsorption.

We finally mention that Verikyos and co-workers[37,38] have also studied the oxidation of C_2H_4 and C_3H_6 on Rh supported on a wide variety of oxides; their studies cannot be directly compared with the present study since catalysts and operating conditions were representative of catalytic converters for the combined removal of NO_x, CO, and HC. They found that the rate of olefin oxidation increased dramatically upon decrease of O_2 concentration below a critical threshold (strictly dependent on the nature of the support), which produced a full reduction of Rh.

4.2. Steam Reforming. The study of methane steam reforming on rhodium has a broad literature basis. It is commonly understood that methane activation is the sole kinetically relevant step. Iglesia and co-workers[30,32,39] verified the independence of CH_4 and C_2H_6 activation from the nature and the amount of the coreactant on clean surfaces. We also found similar pieces of evidence by tests in an annular reactor on Rh.[21,22] Also, in a previous work,[23] the activation of propane was assumed to be the rate determining step of the steam reforming reaction; the experiments confirmed first-order dependence on the fuel concentration and a zero-order dependence on the water concentration.[22]

Differently from the case of methane and propane, the experimental results with propylene showed that the intrinsic rate of steam reforming is enhanced by an increase of water concentration. The CPO experiments at varying O_2 concentration revealed that the rate of H_2 and CO formation depends negligibly on C_3H_6 partial pressure. Moreover, both CPO tests and SR tests confirmed that the onset of steam reforming occurred at relatively high temperature, and Raman measurements showed the presence of C-signals that are missing in the CPO of saturated fuels. We propose that, in the absence of O_2, propylene strongly adsorbs forming different carbon species, which results in surface poisoning. In addition, the steam reforming route is considered to proceed only on free sites. This is a simplified picture that aims at grasping the main observed features, but neglects to describe the nature and chemistry of the inhibiting species that originate from propylene adsorption and do not participate into the reforming process. The following global rate expression is thus proposed:

$$r_{C_3H_6SR} = k_{SR}P_{C_3H_6}(1 - \theta_{C\text{-species}})(1 - \eta_{C_3H_6SR}) \quad (3)$$

where

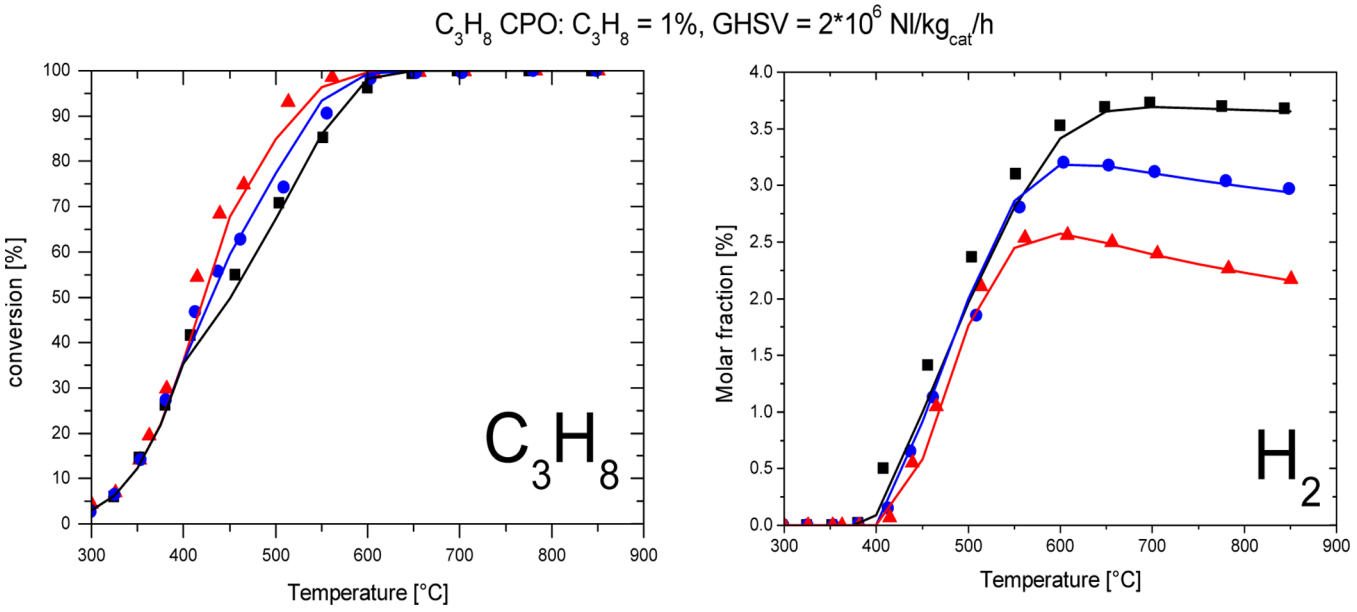

Figure 6. C_3H_8 CPO: Effect of O_2 feed on C_3H_8 conversion (left) and H_2 molar fraction (right). Symbols are experimental data and solid lines are the calculations by the microkinetic model. Operating conditions: C_3H_8 = 1%, (■) O_2 = 1.68%, (●) O_2 = 2.25%, (▲) O_2 = 3%, N_2 to balance, GHSV = 2×10^6 NL/(kg_{cat}/h), atmospheric pressure.

$$1 - \theta_{\text{C-species}} = \frac{1}{1 + K_2 \frac{P_{C_3H_6}}{P_{H_2O}}} \tag{4}$$

The term $(1 - \theta_{\text{C-species}})$ represents the fraction of available active sites, free from carbon poisoning, effectively involved in the steam reforming route. The coverage of C-species was calculated by assuming it as MASI in O_2-free conditions and by considering pseudo-steady-state balance between its production rate via C_3H_6 adsorption and its consumption rate via steam gasification. This can be reasonably explained by considering that H_2O may play a beneficial effect in contrasting the accumulation of surface C-deposits, thus enhancing the rate of steam reforming of the olefin.

The reversibility of steam reforming was respected by introducing the term $(1 - \eta_{C_3H_6SR})$, where $\eta_{C_3H_6SR}$ is the ratio of the experimental reaction quotient $K_{P,SR}$ and the thermodynamic equilibrium constant $K_{EQ,SR}$.[23]

CPO data at varying O_2/C ratios are nicely described by the proposed rate expression. The estimate of parameters are such that the term $(1 - \theta_{\text{C-species}})$, the fraction of surface available for steam reforming, amounts to 0.12 at 400 °C; it increases then to 0.51 at 600 °C and 0.86 at 850 °C.

5. MICROKINETIC ANALYSIS OF PROPANE CPO AND PROPYLENE CPO

In a previous work,[23] a preliminary microkinetic analysis of propane CPO was addressed by coupling a lumped step of propane activation with the C_1 microkinetic scheme developed by Maestri et al.[26] Emphasis was then put on the identification of the probable fragmentation pattern, by comparing the impact of different stoichiometries. It was found that the likely fragmentation path of propane led to the formation of CH_2* species; the formation of CH_3* species would in fact result in a significant production of methane, much larger than that observed in the CPO experiments in the annular reactor.

In this work, we deepen the analysis and we extend it to the case of propylene activation; in particular we focus our attention on reproducing the above-discussed mechanistic features. In the case of propane, two irreversible steps were incorporated corresponding to the oxygen-assisted activation (oxidation, Regime I) and the oxygen-free activation (steam reforming). Assuming that the rate determining step of propane dissociative adsorption (the breaking of the first C−H bond) involves two sites, either O* sites in total oxidation or free sites in steam reforming, the following global stoichiometries and rate expressions were proposed:

$$C_3H_8 + 3* + 2O* \rightarrow 3CH_2* + 2OH* \tag{5}$$

$$r_{C_3H_8Ox} = k_{C_3H_8Ox} \exp\left[-\frac{E_a}{R}\left(\frac{1}{T} - \frac{1}{T_0}\right)\right] P_{C_3H_8} \theta_O{}^2 \tag{6}$$

and

$$C_3H_8 + 5* \rightarrow 3CH_2* + 2H* \tag{7}$$

$$r_{C_3H_8SR} = k_{C_3H_8SR} \exp\left[-\frac{E_a}{R}\left(\frac{1}{T} - \frac{1}{T_0}\right)\right] P_{C_3H_8} \theta_{Rh}{}^2 \tag{8}$$

where θ_o and θ_{Rh} are the coverage of chemisorbed O* and Rh vacancies, respectively.

It is important to note that the global stoichiometries 5 and 7 are written to satisfy the site and atomic balances, and are not representative of elementary steps of the process; instead, the proposed rate expressions 6 and 8 describe the kinetic dependences that are related to the nature of the RDS in total oxidation (dissociative adsorption of propane on two O* sites) and steam reforming (dissociative adsorption of propane on two free sites). As a consequence, the rate of oxidation has a quadratic dependence on oxygen coverage, while the rate of steam reforming has a quadratic dependence on the coverage of free sites. The kinetic parameters incorporated in the two lumped steps were estimated by fitting to the CPO propane data reported by Pagani et al.,[23] after coupling eq 6 and eq 8

Table 2. Rate Equations[a] and Parameter Estimates for the Lumped Steps of C_3H_8 and C_3H_6 Activation Added to the Microkinetic Scheme by Maestri et al.[25,26]

reaction	rate* [mol cm_{Rh}^{-2} s^{-1}]	k_0 [mol atm^{-1} cm_{Rh}^{2} s^{-1}]	E_a [kJ mol^{-1}]
$C_3H_8 + 3* + 2O* \rightarrow 3CH_2* + 2OH*$	$r_{C_3H_8Ox} = k_{C_3H_8Ox} P_{C_3H_8} \theta_O^2$	1.99×10^{-5}	90
$C_3H_8 + 5* \rightarrow 3CH_2* + 2H*$	$r_{C_3H_8SR} = k_{C_3H_8SR} P_{C_3H_8} \theta_{Rh}^2$	1.34×10^{-5}	50
$C_3H_6 + 3* + 3O* \rightarrow 3CH* + 3OH*$	$r_{C_3H_6Ox} = k_{C_3H_6Ox} P_{C_3H_6} \theta_O \theta_{Rh}$	1.13×10^{-4}	20
$C_3H_6 + 3* \rightarrow 3CH_2*$	$r_{C_3H_6SR} = k_{C_3H_6SR} P_{C_3H_6} \theta_{Rh}^2$	2.07×10^{-6}	50

[a]The reaction rate constant (k) is calculated as $k = k_0 \exp[-(E_a/R)((1/T) - (1/T_0))$, where k_0 is the pre-exponential factor estimated at the reference temperature, T_0 = 873 K.

with the C_1 microkintic scheme, and inserting the resulting scheme into the model of the annular reactor.

An activation energy of 90 kJ/mol was found for the oxygen-assisted activation of propane. A lower activation energy for the activation on free sites was found (50 kJ/mol). Nonetheless, the surface coverage is such that this latter route of activation becomes effective only at operating conditions in which O_2 is either totally consumed or mass transfer controlled. Both conditions are associated with the absence of O_2 at the gas–solid interface and on the surface.

An example of the model adequacy to reproduce the CPO data and the macroscopic kinetic dependences is given in Figure 6, where the solid lines represent the simulations with the propane-extended microkinetic scheme. The model reproduces correctly the absence of any O_2-dependence of the low-temperature conversion of propane and describes correctly the shift at higher temperature of the onset of H_2 production at progressively increasing O_2 inlet molar fraction.

To describe propylene CPO, we also introduced two lumped and irreversible steps of activation of the olefin, distinguishing the cases of oxygen-assisted and oxygen-free activation. The formalization of the rate expressions took into account the hypothesis that both oxidation and steam reforming are kinetically controlled by the dissociative adsorption of the olefin on two sites: a vacancy-O* site pair in oxidation (according to Regime II by Chin et al.[32]) and two free sites in steam reforming. Global stoichiometries and rate expressions are as follows:

$$C_3H_6 + 3* + 3O* \rightarrow 3CH* + 3OH* \quad (9)$$

$$r_{C_3H_6Ox} = k_{C_3H_6Ox} \exp\left[-\frac{E_a}{R}\left(\frac{1}{T} - \frac{1}{T_0}\right)\right] P_{C_3H_6} \theta_O \theta_{Rh} \quad (10)$$

and

$$C_3H_6 + 3* \rightarrow 3CH_2* \quad (11)$$

$$r_{C_3H_6SR} = k_{C_3H_6SR} \exp\left[-\frac{E_a}{R}\left(\frac{1}{T} - \frac{1}{T_0}\right)\right] P_{C_3H_6} \theta_{Rh}^2 \quad (12)$$

Additionally, a step of surface poisoning was incorporated; we formalized it as an equilibrated molecular adsorption of propylene on two sites:

$$C_3H_6 + 2* \rightarrow C_3H_6** \quad (13)$$

This represents a terminal step, that is, the C_3H_6** species does not react along the pathway of the microkinetic scheme, and should be regarded as a lumping of carbon species that cumulate on the surface. As a consequence, it is possible that the surface can be fully covered by a monolayer of C_3H_6**. The surface poisoning step required the introduction of additional parameters for the forward and backward steps, including the sticking coefficient of propylene and the activation energy of propylene desorption (we assumed that the adsorption step was not activated). A dependence of desorption energy (that is a dependence of the heat of adsorption) on the coverage of oxygen was incorporated to describe the evidence that the poisoning effect is strongly contrasted by surface oxygen.

The whole set of parameters for the steps involving propylene were similarly estimated by adapting the model of the annular reactor to the available data, after incorporation of the "propylene-extended" C_1 microkinetic scheme. Parameter estimates are reported in Table 2 and 3 and the general adequacy of the model fit is shown in Figure 7 that shows the model response in terms of propylene conversion and H_2 molar fraction at varying O_2/C ratios.

Table 3. Rate Parameters of the Surface Poisoning Step[a]

reaction	s or A [unitless or s^{-1}]	β	E_a [kcal mol^{-1}]
$C_3H_6 + 2* \rightarrow C_3H_6**$	0.5	0	0
$C_3H_6** \rightarrow C_3H_6 + 2*$	5.0×10^{12}	0	30–10 θ_o

[a]The reaction rate constant (k) is calculated as follows:

$$k = \frac{A}{\Gamma_{Rh}^{n-1}} \left(\frac{T}{T_0}\right)^{\beta} \exp\left(-\frac{E_a}{RT}\right)$$

and

$$k = \frac{S}{\Gamma_{Rh}^{n}} \sqrt{\frac{RT}{2\pi MW}} \left(\frac{T}{T_0}\right)^{\beta} \exp\left(-\frac{E_a}{RT}\right)$$

where A is the pre-exponential, s is the sticking coefficient, Γ_{Rh} is the site density (2.49×10^{-09} mol cm^{-2}), n is the reaction order, E_a is the activation energy, R is the ideal gas constant, MW is the molecular weight, and T_0 is the reference temperature (300 K).

The activation energy estimated for propylene oxidative adsorption into CH_2* fragments amounts to 20 kJ/mol, a dramatically lower value than that estimated for propane, in line with the expected stabilization of the transition state of the C–H breaking over O*-vacancy pairs.[32] Instead, the activation energy of propylene on Rh sites is the same as the activation energy of propane steam reforming, which is reasonable given the similarity of the chemical steps involved.

Figure 8 reports the turnover rates predicted by the microkinetic model, divided by the O_2 partial pressure raised to the power of 0.5, as a function of the O_2 inlet concentration. The turnover rates were evaluated on the basis of the calculated

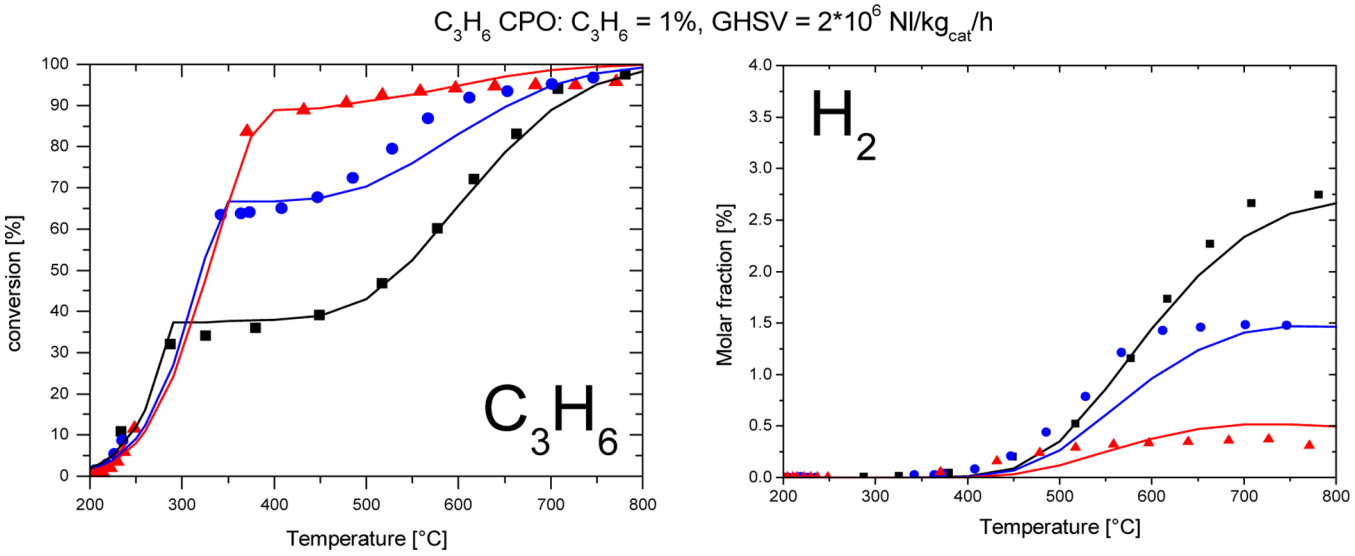

Figure 7. C_3H_6 CPO: Effect of O_2 feed on C_3H_6 conversion (left) and H_2 molar fraction (right). Symbols are experimental data and solid lines are the calculations by the microkinetic model. Operating conditions: C_3H_6 = 1%, (■) O_2 = 1.7%, (●) O_2 = 3%, (▲) O_2 = 4%, N_2 to balance; GHSV = 2×10^6 NL/(kg_{cat}/h), atmospheric pressure.

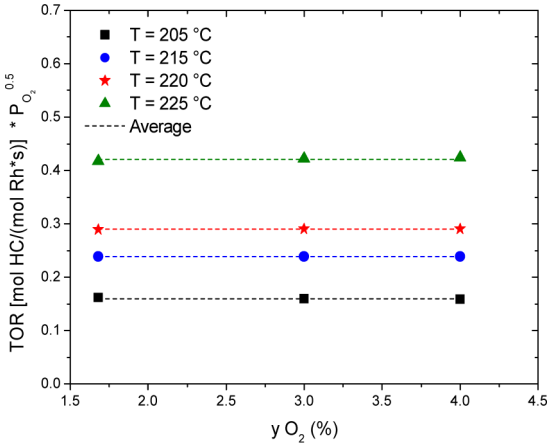

Figure 8. Calculated turnover rates multiplied by O_2 partial pressure raised to the power of 0.5 for the C_3H_6 CPO experiments at increasing O_2 inlet molar fraction.

values of C_3H_6 conversion in the differential regime (T < 250 °C). Given the flat trends of TOR with increasing O_2, it is evident that the microkinetic model predicts a reaction order of −0.5 for O_2 partial pressure, which is not consistent with our experimental findings (the observed reaction order is −1) and the kinetic dependences of Regime 2 by Iglesia and co-workers. Such a discrepancy turns out to be related to the description of the O/Rh interaction. In fact, if the hypothesis of irreversible O_2* dissociation into O* is removed, being replaced by equilibrium of O_2* dissociation, the formalization of Regime 2, that is, activation of C_3H_6 on a *-O* site pair, changes in the following rate expression:

$$r_{C_3H_6Ox} = \frac{k_{C_3H_6Ox} P_{C_3H_6} P_{O_2}^{0.5}}{(1 + \sqrt{K_{O_2ads} P_{O_2}})^2} \quad (14)$$

This expression reflects the actual response of the present microkinetic scheme, wherein the heat of chemisorption of O* is such that O_2 dissociation is always equilibrated.

The impact of this inaccuracy on the final prediction of the reactor model is only minor, but the finding has interesting implications since it suggests that the energetics of the interaction between O_2 and Rh may deserve further investigation and refinement.

A final comment regards the inclusion of the lumped adsorption step of propylene (eq 13), which globally represents the carbon poisoning phenomenon observed in the CPO runs after complete consumption of oxygen and in the SR runs. While the microkinetic scheme does not include a coke-chemistry (formation, growth, and consumption of C-species such as those originated from cracking of adsorbed hydrocarbon intermediates), still this strategy allowed a description of the poisoning phenomenon as a partial occupation of Rh sites by propylene (and associated carbon species), which weakens at increasing temperature in line with the thermochemistry of an adsorption equilibrium. The quantification of this step is such that the intrinsic rate of propylene steam reforming over the available surface is greater than the rate of propane steam reforming, as reasonably expected considering the higher chemical reactivity of an olefin compared with that of the corresponding saturated hydrocarbon.

6. CONCLUSIONS

The present kinetic investigation showed that the partial oxidation of propylene is an indirect process, similar to the partial oxidation of methane or propane. Deep oxidation uniquely occurs at the lowest temperatures; steam reforming is a consecutive route, responsible for synthesis gas production, active at temperatures higher than 500 °C.

Unique kinetic features were found; however, compared with the CPO of the saturated light hydrocarbons, the oxidation of propylene occurs according to the typical dependences of a Regime 2 (according to the nomenclature introduced by Iglesia and co-workers), wherein the rate determining step is the breaking of a C−H bond over a highly reactive vacancy-O* site pair and O* is not equilibrated with O_2* species. Regime 2 results in a negative dependence on O_2 partial pressure, a quadratic dependence on the fuel concentration, and a

significant increase of the turnover rate. Notably, again referring to the nomenclature introduced by Iglesia and co-workers, the oxidation of CH_4 and C_3H_8 on Rh occurs according to a Regime 1 (C−H breaking on an oxygen-saturated surface). It is thus concluded that the stronger affinity of the olefin with the Rh surface establishes an effective competition with O_2 adsorption (which is not the case of saturated hydrocarbons), beneficial to the rate of oxidation since it makes available highly reactive vacancy-O* site-pairs.

In the absence of O_2, the reactivity of propylene is believed to produce instead a poisoning effect on steam reforming which is relieved at increasing temperature. Steam reforming is thus hindered at temperatures below 500 °C, and higher temperatures are necessary compared with methane and propane to observe the effective production of CO and H_2. Thus, in the case of O* free surfaces, the adsorption of propylene (and the formation of additional intermediates and C-species) has a negative impact on propylene activation.

Both the oxidation and steam reforming of propylene can be quantitatively described by means of molecular rate expressions, which explicitly account for the observed kinetic dependences. This approach leads to the development of a relatively simple and flexible kinetic scheme that describes well the effects observed within the experimental campaign, similarly to the results obtained from the kinetic investigation of CH_4 CPO and C_3H_8 CPO. The molecular kinetic scheme, herein proposed, is thus especially suitable for modeling applications; for instance, to evaluate the impact of the heterogeneous conversion of propylene on the thermal behavior and on the product composition of a propane CPO reformer.

In addition, in this work we verified the adequacy of an alternative approach based on the coupling of lumped steps of activation of the olefin to C_1 surface species with our C_1-microkinetic scheme, previously developed. This approach was tested both for propane CPO and propylene CPO. We found that the oxidation (in Regime 1) and the steam reforming of propane are accurately described by simply incorporating the irreversible steps for the oxygen-assisted and oxygen-free activation of the C_3 fuel; the final kinetic scheme confirms that O* coverage is close to 1 as long as O_2 is present in the gas−solid interface and the conversion of propane is independent of O_2 concentration in the feed.

In the case of propylene, three steps were incorporated into the microkinetic scheme: the irreversible activation on vacancy-O* pairs, the irreversible activation on an O*-free surface, and the reversible adsorption Rh sites. In this way we could nicely describe the sluggish conversion curve of propylene, with the poisoning effect of propylene on steam reforming. In addition, the O/Rh interaction turned out to be the critical parameter of the microkinetic analysis to correctly describe the observed quadratic dependence on propylene concentration and the negative dependence on O_2 concentration. However, the propylene-extended microkinetic model allowed quantification of the coverage of propylene and propylene-derived intermediates that block the surface under steam reforming conditions, suggesting that the intrinsic rate of propylene activation on the available Rh surface is indeed higher than that of propane, consistent with the high reactivity in oxidation.

AUTHOR INFORMATION

Corresponding Authors

*E-mail: alessandra.beretta@polimi.it.

*E-mail: gianpiero.groppi@polimi.it.

Notes

The authors declare no competing financial interest.

REFERENCES

(1) Degenstein, N. J.; Subramanian, R.; Schmidt, L. D. Partial oxidation of *n*-hexadecane at short contact times: Catalyst and washcoat loading and catalyst morphology. *Appl. Catal., A* **2006**, *305* (2), 146−159.

(2) Schmidt, L. D.; Balonek, C. M.; Colby, J. L.; Persson, N. E. Rapid ablative pyrolysis of cellulose in an autothermal fixed-bed catalytic reactor. *Chemsuschem* **2010**, *3* (12), 1355−1358.

(3) Diehm, C.; Kaltschmitt, T.; Deutschmann, O. Hydrogen production by partial oxidation of ethanol/gasoline blends over Rh/Al_2O_3. *Catal. Today* **2012**, *197* (1), 90−100.

(4) Donazzi, A.; Maestri, M.; Michael, B. C.; Beretta, A.; Forzatti, P.; Groppi, G.; Tronconi, E.; Schmidt, L. D.; Vlachos, D. G. Microkinetic modeling of spatially resolved autothermal CH_4 catalytic partial oxidation experiments over Rh-coated foams. *J. Catal.* **2010**, *275* (2), 270−279.

(5) Dreyer, B. J.; Lee, I. C.; Krummenacher, J. J.; Schmidt, L. D. Autothermal steam reforming of higher hydrocarbons: *n*-decane, *n*-hexadecane, and JP-8. *Appl. Catal., A* **2006**, *307* (2), 184−194.

(6) Krummenacher, J. J.; West, K. N.; Schmidt, L. D. Catalytic partial oxidation of higher hydrocarbons at millisecond contact times: decane, hexadecane, and diesel fuel. *J. Catal.* **2003**, *215* (2), 332−343.

(7) Schmidt, L. D.; Panuccio, G. J.; Dreyer, B. J. A comparison of the catalytic partial oxidation of C-1 to C-16 normal paraffins. *AIChE J.* **2007**, *53* (1), 187−195.

(8) Tavazzi, I.; Beretta, A.; Groppi, G.; Donazzi, A.; Maestri, M.; Tronconi, E.; Forzatti, P. Catalytic partial oxidation of CH_4 and C_3H_8: experimental and modeling study of the dynamic and steady state behavior of a pilot-scale reformer. *Stud. Surf. Sci. Catal.* **2007**, *167*, 319−324.

(9) Williams, K. A.; Horn, R.; Schmidt, L. D. Performance of mechanisms and reactor models for methane oxidation on Rh. *AIChE J.* **2007**, *53* (8), 2097−2113.

(10) Donazzi, A.; Pagani, D.; Lucotti, A.; Tommasini, M.; Beretta, A.; Groppi, G.; Castiglioni, C.; Forzatti, P. Annular reactor testing and Raman surface characterization in the CPO of methane and propylene. *Appl. Catal. A: Gen.* **2013**.

(11) Hartmann, M.; Lichtenberg, S.; Hebben, N.; Zhang, D.; Deutschmann, O. Experimental investigation of catalytic partial oxidation of model fuels under defined constraints. *Chem. Ing. Tech.* **2009**, *81* (7), 909−919.

(12) Hartmann, M.; Maier, L.; Minh, H. D.; Deutschmann, O. Catalytic partial oxidation of iso-octane over rhodium catalysts: An experimental, modeling, and simulation study. *Combust. Flame* **2010**, *157* (9), 1771−1782.

(13) Maier, L.; Hartmann, M.; Tischer, S.; Deutschmann, O. Interaction of heterogeneous and homogeneous kinetics with mass and heat transfer in catalytic reforming of logistic fuels. *Combust. Flame* **2011**, *158* (4), 796−808.

(14) Korup, O.; Schlögl, R.; Horn, R. Carbon formation in catalytic partial oxidation of methane on platinum: Model studies on a polycrystalline Pt foil. *Catal. Today* **2012**, *181* (1), 177−183.

(15) Korup, O.; Goldsmith, C. F.; Weinberg, G.; Geske, M.; Kandemir, T.; Schlögl, R.; Horn, R. Catalytic partial oxidation of methane on platinum investigated by spatial reactor profiles, spatially resolved spectroscopy, and microkinetic modeling. *J. Catal.* **2013**, *297* (0), 1−16.

(16) Quiceno, R.; Perez-Ramirez, J.; Warnatz, J.; Deutschmann, O. Modeling the high-temperature catalytic partial oxidation of methane over platinum gauze: Detailed gas-phase and surface chemistries coupled with 3D flow field simulations. *Appl. Catal. A: Gen.* **2006**, *303* (2), 166−176.

(17) Mhadeshwar, A. B.; Vlachos, D. G. A catalytic reaction mechanism for methane partial oxidation at short contact times, reforming, and combustion, and for oxygenate decomposition and

oxidation on platinum. *Ind. Eng. Chem. Res.* **2007**, *46* (16), 5310−5324.
(18) Donazzi, A.; Livio, D.; Maestri, M.; Beretta, A.; Groppi, G.; Tronconi, E.; Forzatti, P. Synergy of Homogeneous and Heterogeneous Chemistry Probed by in Situ Spatially Resolved Measurements of Temperature and Composition. *Angew. Chem., Int. Ed.* **2011**, *50* (17), 3943−3946.
(19) Livio, D.; Donazzi, A.; Beretta, A.; Groppi, G.; Forzatti, P. Experimental and modeling analysis of the thermal behavior of an autothermal C_3H_8 catalytic partial oxidation reformer. *Ind. Eng. Chem. Res.* **2012**, *51* (22), 7573−7583.
(20) Beretta, A.; Bruno, T.; Groppi, G.; Tavazzi, I.; Forzatti, P. Conditioning of Rh/α-Al_2O_3 catalysts for H_2 production via CH_4 partial oxidation at high space velocity. *Appl. Catal. B: Environ.* **2007**, *70* (1−4), 515−524.
(21) Donazzi, A.; Beretta, A.; Groppi, G.; Forzatti, P. Catalytic partial oxidation of methane over a 4% Rh/a-Al_2O_3 catalyst Part I: Kinetic study in annular reactor. *J. Catal.* **2008**, *255* (2), 241−258.
(22) Donazzi, A.; Beretta, A.; Groppi, G.; Forzatti, P. Catalytic partial oxidation of methane over a 4% Rh/a-Al_2O_3 catalyst Part II: Role Of CO_2 reforming. *J. Catal.* **2008**, *255* (2), 259−268.
(23) Pagani, D.; Livio, D.; Donazzi, A.; Beretta, A.; Groppi, G.; Maestri, M.; Tronconi, E. A kinetic analysis of the partial oxidation of C_3H_8 over a 2% Rh/Al_2O_3 catalyst in annular microreactor. *Catal. Today* **2012**, *197* (1), 265−280.
(24) Ibashi, W.; Groppi, G.; Forzatti, P. Kinetic measurements of CH_4 combustion over a 10% PdO/ZrO_2 catalyst using an annular flow microreactor. *Catal. Today* **2003**, *83* (1−4), 115−129.
(25) Shah, R. K.; London, A. L. *Laminar Flow Forced Convection in Ducts*. Academic Press: New York, 1978.
(26) Maestri, M.; Vlachos, D. G.; Beretta, A.; Groppi, G.; Tronconi, E. A C_1 microkinetic model for the conversion of methane to syngas on Rh/Al_2O_3. *AIChE J.* **2009**, *55*, 993−1008.
(27) Maestri, M.; Reuter, K. Molecular-level understanding of WGS and reverse WGS reactions on Rh through hierarchical multiscale approach. *Chem. Eng. Sci.* **2012**, *74* (0), 296−299.
(28) Mhadeshwar, A. B.; Vlachos, D. G. Hierarchical multiscale mechanism development for methane partial oxidation and reforming and for thermal decomposition of oxygenates on Rh. *J. Phys. Chem. B* **2005**, *109* (35), 16819−16835.
(29) Bionanlytical Microfluidics Program. http://navier.engr.colostate.edu/~dandy/code/code-4/index.html (accessed 2013).
(30) García-Diéguez, M.; Chin, Y. H. C.; Iglesia, E. Catalytic reactions of dioxygen with ethane and methane on platinum clusters: Mechanistic connections, site requirements, and consequences of chemisorbed oxygen. *J. Catal.* **2012**, *285* (1), 260−272.
(31) Maestri, M.; Vlachos, D. G.; Beretta, A.; Forzatti, P.; Groppi, G.; Tronconi, E. Dominant reaction pathways in the catalytic partial oxidation of methane on Rh. *Top. Catal.* **2009**, *52*, 1983−1988.
(32) Chin, Y.-H.; Buda, C.; Neurock, M.; Iglesia, E. Reactivity of chemisorbed oxygen atoms and their catalytic consequences during CH_4−O_2 catalysis on supported Pt clusters. *J. Am. Chem. Soc.* **2011**, *133* (40), 15958−15978.
(33) Wei, J. M.; Iglesia, E. Structural requirements and reaction pathways in methane activation and chemical conversion catalyzed by rhodium. *J. Catal.* **2004**, *225* (1), 116−127.
(34) Chin, Y. H.; Buda, C.; Neurock, M.; Iglesia, E. Selectivity of chemisorbed oxygen in C-H bond activation and CO oxidation and kinetic consequences for CH_4−O_2 catalysis on Pt and Rh clusters. *J. Catal.* **2011**, *283* (1), 10−24.
(35) Calhorda, M. J.; Lopes, P. E. M.; Friend, C. M. Theoretical studies of ethylene adsorption and oxidation on clean and oxygen covered rhodium (111). *J. Mol. Catal A: Chem.* **1995**, *97* (3), 157−171.
(36) Xu, X.; Friend, C. M. Partial oxidation without allylic carbon-hydrogen bond activation: The conversion of propene to acetone on rhodium(111)-p(2×1)-O. *J. Am. Chem. Soc.* **1991**, *113* (18), 6779−6785.
(37) Kotsifa, A.; Kondarides, D. I.; Verykios, X. E. A comparative study of the selective catalytic reduction of NO by propylene over supported Pt and Rh catalysts. *Appl. Catal. B: Environ.* **2008**, *80* (3−4), 260−270.
(38) Pliangos, C.; Yentekakis, I. V.; Papadakis, V. G.; Vayenas, C. G.; Verykios, X. E. Support-induced promotional effects on the activity of automotive exhaust catalysts: 1. The case of oxidation of light hydrocarbons (C_2H_4). *Appl. Catal. B: Environ.* **1997**, *14* (3−4), 161−173.
(39) Wei, J. M.; Iglesia, E. Isotopic and kinetic assessment of the mechanism of reactions of CH_4 with CO_2 or H_2O to form synthesis gas and carbon on nickel catalysts. *J. Catal.* **2004**, *224* (2), 370−383.